THE JOURNAL OF BIOLOGICAL CHEMISTRY VOL. 286, NO. 50, pp. 43334–43342, December 16, 2011

Structural Basis of Phosphoinositide Binding to Kindlin-2 Protein Pleckstrin Homology Domain in Regulating Integrin Activation*[S]

Received for publication, August 18, 2011, and in revised form, October 18, 2011 Published, JBC Papers in Press, October 26, 2011, DOI 10.1074/jbc.M111.295352

Jianmin Liu[‡1], **Koichi Fukuda**[‡1,2], **Zhen Xu**[‡1], **Yan-Qing Ma**[‡], **Jamila Hirbawi**[‡], **Xian Mao**[§], **Chuanyue Wu**[¶], **Edward F. Plow**[‡3], **and Jun Qin**[‡§4]

From the [‡]*Department of Molecular Cardiology, Lerner Research Institute, Cleveland Clinic, Cleveland, Ohio 44195, the* [§]*Cleveland Center for Structural and Membrane Biology, Cleveland, Ohio 44106, and the* [¶]*Department of Pathology, University of Pittsburgh, Pittsburgh, Pennsylvania 15261*

Background: Kindlin-2 is a key regulator of integrin activation.
Results: Kindlin-2 contains a PH domain with a distinct binding pocket for phosphatidylinositol-(3,4,5)-trisphosphate (PIP3) that promotes talin-mediated integrin activation.
Conclusion: PIP3-mediated membrane binding of kindlin-2 is crucial for the cooperation of kindlin-2 with talin in activating integrin.
Significance: Learning how kindlin-2 functions is crucial for understanding the integrin-mediated cell adhesion.

Kindlins are a subclass of FERM-containing proteins that have recently emerged as key regulators of integrin receptor activation and signaling. As compared with the conventional FERM domain, the kindlin FERM domain contains an inserted pleckstrin homology (PH) domain that recognizes membrane phosphoinositides, including phosphatidylinositol 4,5-bisphosphate (PIP2) and phosphatidylinositol 3,4,5-trisphosphate (PIP3). Using NMR spectroscopy, we show that PIP3 site-specifically binds to kindlin-2 PH with substantial chemical shift changes that are much larger than PIP2. This suggests an enhanced association of kindlin-2 with membrane as mediated by PIP3 upon its conversion from PIP2 by phosphoinositide-3 kinase, a known regulator of integrin activation. We determined the NMR structure of the kindlin-2 PH domain bound to the head group of PIP3, inositol 1,3,4,5-tetraphosphate (IP4). The structure reveals a canonical PH domain fold, yet with a distinct IP4 binding pocket that appears highly conserved for the kindlin family members. Functional experiments demonstrate that although wild type kindlin-2 is capable of cooperating with integrin activator talin to induce synergistic integrin $\alpha_{IIb}\beta_3$ activation, this ability is significantly impaired for a phosphoinositide binding-defective kindlin-2 mutant. These results define a specific PIP3 recognition mode for the kindlin PH domain. Moreover, they shed light upon a mechanism as to how the PH domain mediates membrane engagement of kindlin-2 to promote its binding to integrin and cooperation with talin for regulation of integrin activation.

The integrin-mediated interaction between cell and extracellular matrix (ECM)[5] is a fundamental process in a variety of physiological and pathological responses (1). Integrins are transmembrane receptors that function by binding to a variety of ECM ligands such as fibrinogen or fibronectin while connecting to the intracellular cytoskeleton, allowing dynamic regulation of cell-ECM adhesion and migration. A distinct feature of integrins is their activation, which occurs via a so-called inside-out process, *i.e.* upon cellular stimulation, an intracellular signal propagates through the integrin cytoplasmic face to its extracellular domain, inducing a long range conformational change in the receptor for high affinity ECM ligand binding (1–4). Talin, a major cytoskeletal adaptor, is known to play a pivotal role in initiating such conformational change by binding to the integrin β cytoplasmic tail (CT) (5–8). However, recent genetic and cell biological analyses have shown that a family of cytoskeletal adaptors called kindlins can also bind β integrin CTs and critically regulate integrin activation (9–16). In particular, kindlin-2, which is highly concentrated at integrin-rich cell-ECM adhesions (17), was found to dramatically enhance

* This work was supported, in whole or in part, by National Institutes of Health Grants GM62823 (to J. Q.), P01 HL073311 (to E. F. P.), and GM65188 and DK54639 (to C. W.). This work was also supported by American Heart Association Scientist Development Grant 10SDG2610277 (to Y. M.).
[S] The on-line version of this article (available at http://www.jbc.org) contains supplemental Table S1 and Figs. S1–S5.
The atomic coordinates and structure factors (code 2LKO) have been deposited in the Protein Data Bank, Research Collaboratory for Structural Bioinformatics, Rutgers University, New Brunswick, NJ (http://www.rcsb.org/). The chemical shift data were deposited in the Biological Magnetic Resonance Bank (accession number 18002).
[1] These authors contributed equally to this work.
[2] Supported by the Kirschstein-National Research Service Award (NRSA) research training grant through the National Institutes of Health.
[3] To whom correspondence may be addressed: Dept. of Molecular Cardiology, Lerner Research Institute, Cleveland Clinic, 9500 Euclid Ave., Cleveland, OH 44195. Tel.: 216-445-8200; Fax: 216-445-8204; E-mail: plowe@ccf.org.
[4] To whom correspondence may be addressed: Dept. of Molecular Cardiology, Lerner Research Institute, Cleveland Clinic, 9500 Euclid Ave., Mail code NB20, Cleveland, OH 44195. Tel.: 216-444-5392; Fax: 216-445-1466; E-mail: qinj@ccf.org.

[5] The abbreviations used are: ECM, extracellular matrix; CT, cytoplasmic tail; FERM, four-point-one, ezrin, radixin, moesin; HSQC, heteronuclear single quantum coherence; IP3, inositol 1,4,5-triphosphate; IP4, inositol 1,3,4,5-tetraphosphate; PIP2, phosphatidylinositol 4,5-diphosphate; PIP3, phosphatidylinositol 3,4,5-triphosphate; K2, Kindlin-2; PH domain, pleckstrin homology domain; EGFP, enhanced green fluorescent protein.

the talin-mediated integrin $\alpha_{IIb}\beta_3$ activation (12–14). Biochemical analysis demonstrated that the kindlin-2 binding site on integrin β3 CT does not overlap with that for talin (9, 12, 13), suggesting that kindlin-2 likely acts as the highly sought co-activator of integrins (18, 19). However, how the kindlin-2 localizes to the integrin site and cooperates with talin for activating integrins remains poorly understood.

Kindlins are a subclass of FERM (four-point-one, ezrin, radixin, moesin) domain proteins that contain F1, F2, and F3 subdomains. Like talin, kindlins also have an F0 domain prior to the FERM domain (see Fig. 1*A*) and their F3 domain binds to integrin β CTs (9, 12, 13). However, distinct from talin, kindlins have a pleckstrin homology (PH) domain inserted in the middle of F2 domain (see Fig. 1*A*). We previously demonstrated that the inserted PH domain binds to phosphoinositides including phosphatidylinositol 4,5-diphosphate (PIP2) and phosphatidylinositol 3,4,5-triphosphate (PIP3) (20), both of which are known regulators of integrin-mediated cell adhesion (21, 22). However, the structural basis for the phosphoinositide/kindlin PH recognition and how it may regulate the kindlin function remain elusive.

In this study, we have undertaken a detailed comparative analysis of the kindlin-2 PH domain (hereafter referred to as K2-PH) binding to PIP2 and PIP3. NMR-based chemical shift mapping demonstrates that PIP3 induced much larger chemical shift changes of K2-PH than PIP2, suggesting an enhanced membrane association of kindlin-2 upon conversion of PIP2 to PIP3 by phosphoinositide-3 kinase (PI3K), a crucial enzyme that has been implicated in regulating the function of kindlin-2 and integrin activation (20). Using triple resonance NMR spectroscopy, we have determined the solution structure of the K2-PH domain in complex with the head group (inositol 1,3,4,5-tetraphosphate (IP4)) of PIP3. The structure contains a distinct positively charged IP4 binding pocket that appears highly conserved in the kindlin family. Disruption of the phosphoinositide binding to the PH domain dramatically reduces the ability of kindlin-2 to synergize with talin for activating integrin $\alpha_{IIb}\beta_3$, demonstrating that the PIP3 binding to kindlin-2 is crucial for its integrin co-activator function. Overall, the results provide significant molecular insight into a specific phosphoinositide-mediated membrane localization of kindlin-2 and demonstrate that such localization is a crucial step for cooperation with talin for regulating integrin activation.

EXPERIMENTAL PROCEDURES

Protein Expression, Purification, and Mutagenesis—The expression plasmid for the human K2-PH domain (residues 367–500) was generated using a pET15b vector (Novagen), as described previously (20). The unlabeled, uniformly ^{15}N-labeled, and ^{15}N/^{13}C-labeled hexahistidine-tagged recombinant K2-PH proteins were expressed in *Escherichia coli* and purified from the bacterial cell lysate on a nickel affinity chromatography column followed by a Resource-S cation-exchange column and a HiLoad 16/60 Superdex 200 gel filtration column (all from GE Healthcare). The amino-terminal hexahistidine tag of the K2-PH proteins was removed by thrombin cleavage, and K2-PH was eluted from gel filtration in monomeric form. The amino acid substitutions of the K2-PH proteins were carried out by PCR-based mutagenesis experiments using the QuikChange site-directed mutagenesis kit (Stratagene, La Jolla, CA) with appropriate primer sets. The mutant proteins of K2-PH were expressed and purified as for the wild type. All the DNA constructs were verified by sequencing.

NMR Data Collection and Analysis—Uniformly ^{15}N-labeled or ^{15}N/^{13}C-labeled K2-PH protein (1 mM) was dissolved in 10 mM Hepes, pH 6.8, 50 mM NaCl, 2 mM DTT with or without 2 mM IP4 (Echelon Bioscience Inc., Salt Lake City, UT, catalogue number Q-1345) in 90% H_2O/10% (v/v) D_2O or 99.96% D_2O. Inositol 1,4,5-triphosphate (IP3, catalogue number Q-0145) was also used for chemical shift mapping analysis. All NMR experiments were carried out at 30 °C on Bruker Avance spectrometers (600- and 900-MHz ^{1}H operating frequencies). The resonance assignments of ^{15}N/^{13}C-labeled K2-PH bound to IP4 (at 1:1.2 molar ratio) in 90% H_2O/10% (v/v) D_2O were carried out using standard triple resonance experiments (23). Nuclear Overhauser effect (NOE) data for K2-PH structural calculations were obtained from a [^{1}H-^{15}N] NOESY spectrum (τ_m = 120 ms) and [^{1}H-^{13}C] NOESY (τ_m = 120 ms). The resonance assignments of IP4 bound with ^{15}N/^{13}C-labeled K2-PH were made by two-dimensional ^{14}N/^{12}C-filtered total correlation spectroscopy spectra (τ_m = 15 and 60 ms, respectively) and the comparison of the one-dimensional spectra between the bound and free IP4 (see the supplemental material). Intermolecular NOEs between K2-PH and IP4 were obtained using three-dimensional ^{15}N/^{13}C filtered (F1) [^{1}H-^{13}C] NOESY-HSQC in 99.96% D_2O (τ_m = 200 ms). All the NMR data were processed using NMRPipe (24) and analyzed with Sparky (T. D. Goddard and D. G. Kneller, University of California, San Franciso, CA). For chemical shift mapping, weighted chemical shift changes were calculated using the equation

$$\Delta\delta_{obs[HN,N]} = ([\Delta\delta_{HN}W_{HN}]^2 + [\Delta\delta_N W_N]^2)^{1/2} \quad \text{(Eq. 1)}$$

where $W_{HN} = 1$ and $W_N = 0.154$ are weighting factors based on the gyromagnetic ratios of ^{1}H and ^{15}N.

Structure Determination—Structure calculations for the K2-PH·IP4 complex were performed in two steps. First, the bound form of K2-PH was calculated using ARIA2.2 (25) based on >95% unambiguously assigned NOEs, which generated the initial K2-PH model. The best structure was selected based on the lowest overall energy, and more ambiguous NOEs were assigned based on this structure. These NOEs and dihedral restraints (ϕ/ψ) obtained from the TALOS database (26) were added to the original NOE list for further refining the structure using Xplor-NIH (27). The complex structure was calculated by including intermolecular NOEs between K2-PH and IP4. Among the intermolecular NOEs observed, the assignments of seven NOEs from ^{15}N/^{13}C-filtered NOESY (K383ϵ, IP4 H2; K383ϵ, IP4 H3; K383δ, IP4 H2; K393ϵ, IP4 H3; K408ϵ, IP4 H2; K408ϵ, IP4 H3; and K408δ, IP4 H2) and two NOEs from ^{15}N NOESY (L389H^N, IP4 H6 and G391H^N, IP4 H2) are unambiguous, and the constraints generated from them defined the spatial position and orientation of the IP4 molecule with the decent convergence in the initial complex structure calculation cycle. The ambiguity of other intermolecular NOEs was resolved by referring to the initial calculated structure ensemble and chem-

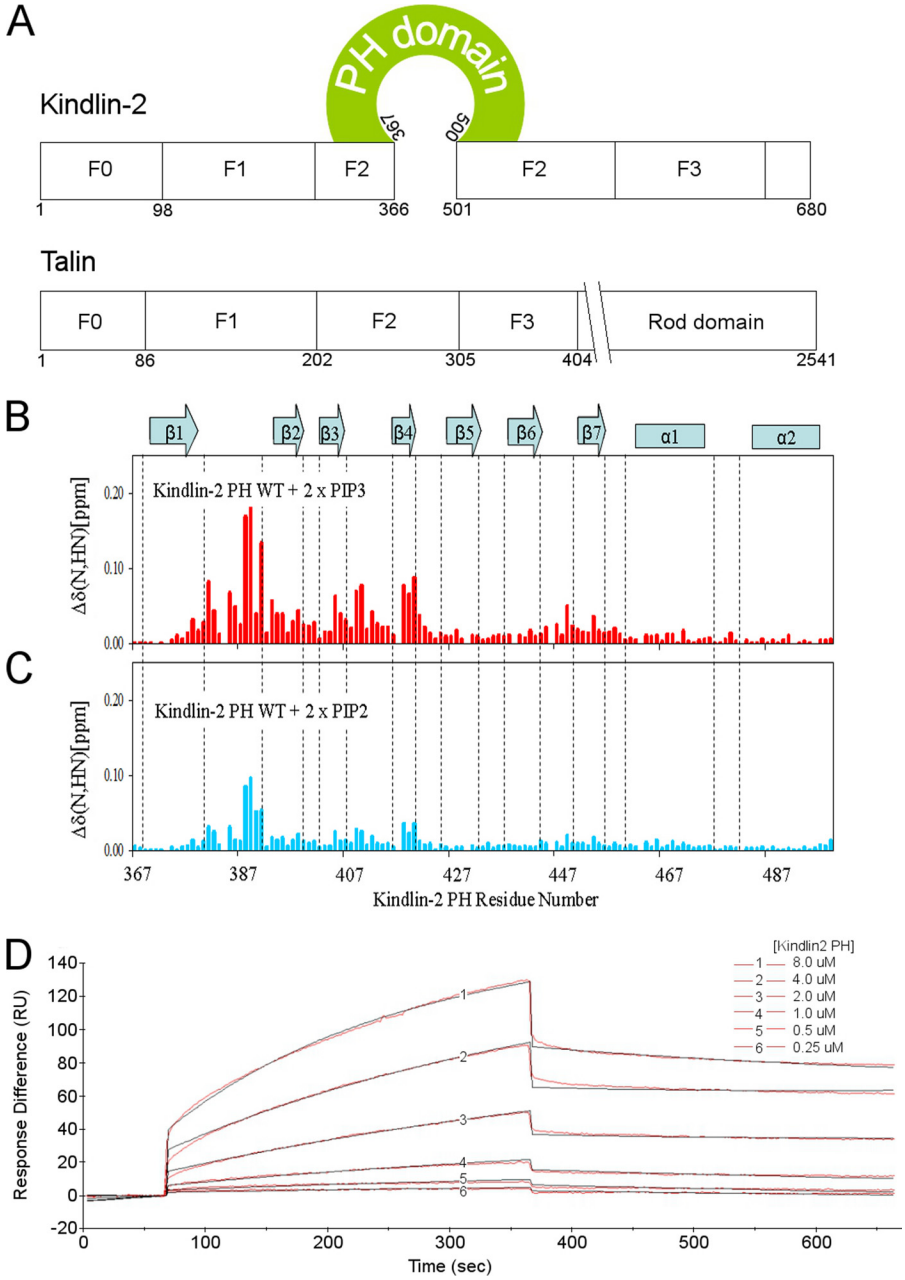

FIGURE 1. **Kindlin-2 FERM domain contains a distinct inserted PH domain that interacts with phosphoinositides.** *A*, *top*, diagram of the domain structure of kindlin-2 and the location of the PH domain. The residue numbers for the domain boundaries are indicated based on the known structure data. *Bottom*, diagram of the domain structure of the talin FERM domain. *B* and *C*, chemical shift perturbation profile of the kindlin-2 PH domain upon IP4 binding (*B*, *red*) and upon IP3 binding (*C*, *blue*). The secondary structure regions of the kindlin-2 PH domain are highlighted by *arrows* and *rectangles* with *vertical dots*. *D*, representative real-time sensorgrams of the binding interaction between kindlin-2 PH domain and the biotinylated phosphatidylinositol 3,4,5-triphosphate by surface plasmon resonance analysis. The real-time binding curves were fitted very well using a global fitting algorithm to a 1:1 binding model, resulting in the $K_D = 2.12 \pm 0.19$ μM. Note that the affinity might be lower because the binding did not reach the complete steady state, which was prevented by very slow association and possible aggregation at longer injection times. *RU*, resonance units.

ical shift perturbation in [^{1}H-^{15}N] HSQC and [^{1}H-^{13}C] HSQC, and the assignments were further confirmed by detailed mutagenesis studies. The total 19 intermolecular constraints were used in the complex structural calculation. The flag of DIHE (the energy term of dihedral angle) was turned on in the Xplor annealing protocol, which treated the inositol ring as a rigid body. At the final stage of the structure refinements, hydrogen-bond restraints were incorporated for regular secondary structures including α-helices and β-sheets.

Phosphoinositide Binding Studies—Direct binding interactions between K2-PH protein and phosphoinositides were measured by a Biacore 3000 instrument (GE Healthcare). All the experiments were performed at 25 °C using a filtered/degassed running buffer consisting of 10 mM Hepes, pH 7.4, 150 mM NaCl, 0.005% (v/v) surfactant P20, and 3 mM EDTA. Biotinylated IP4 (catalogue number C-39B6a) or biotinylated IP3 (catalogue number C45B6a) (Echelon Bioscience Inc.) was captured to yield ~130 resonance units on the flow cell 2 of a

streptavidin-coated sensor chip SA (GE Healthcare) according to the manufacturer's protocol. The flow cell 1 was used as a reference cell by not capturing biotinylated lipid, and sensorgrams showing specific binding were generated by subtracting the signals of the flow cell 1 from those of the flow cell 2. The K2-PH solution was injected at various concentrations ranging from 0.25 to 8.0 μM over the immobilized biotinylated lipid at a flow rate of 10 μl/min. The sensor chip was regenerated between each injection by flowing a washing solution (0.05% SDS) in the running buffer at 50 μl/min for 15 s. The data were analyzed by BIAevaluation version 4.0.1 (Biacore). The data measurements were performed in duplicate.

Integrin $\alpha_{IIb}\beta_3$ Activation Assay—Activation of integrin $\alpha_{IIb}\beta_3$ was assessed as described previously (12) using PAC1, an antibody specific for the active conformation of the integrin. EGFP-fused Kindlin-2 WT or its mutants were co-transfected with Talin-H into $\alpha_{IIb}\beta_3$-CHO (A5) cells using Lipofectamine 2000 (Invitrogen). Cells were collected 24 h after transfection, treated with 10 μg/ml PAC1 IgM- and Alexa Fluor 633 goat anti-mouse IgM-conjugated antibody, and fixed with 4% paraformaldehyde. Integrin activation was analyzed by flow cytometry (FACS) measuring the median fluorescence intensity of PAC1 binding. Background staining due to secondary antibody alone was subtracted from all values. To obtain relative median fluorescence intensity values, median fluorescence intensities of PAC1 binding were normalized based on PAC1 binding to cells transfected with EGFP vector alone.

TABLE 1
Structural statistics for Kindlin-2 PH domain·IP4 complex

Summary of restraints	
Kindlin-2 PH intra molecular restraints	
Intraresidue (*i*, *i*)	666
Sequential (*i*, *i*+1)	625
Medium (*i*, 2–4)	206
Long range (*i*, >4)	304
Total	1820
Dihedral angles ϕ, ψ	100, 100
K2 PH/IP4 intermolecular restraints	19
Deviation from restraints	
All distance restraints, Å	0.03270 ± 0.00493
Dihedral restraints, degree	0.76308 ± 0.07553
Residues in allowed regions of Ramachandran plot[a,b]	97.3%
Deviation from idealized geometry	
Bonds, Å	0.00569 ± 0.0002
Angles, degree	0.78439 ± 0.02451
Improper angles, degree	1.53520 ± 0.01351
EL-J (kcal/mol)[b]	−502.788 ± 14.906
r.m.s.d[c] from average structure[b]	
Backbone, Å	1.172 ± 0.168
All heavy atoms, Å	1.675 ± 0.227

[a] Calculated from Procheck-NMR.
[b] Residues: 375–500 of total 20 simulated annealing structures.
[c] r.m.s.d., root mean square difference.

RESULTS

Characterization of the Binding of Kindlin-2 PH Domain to PIP2 and PIP3—Previous biochemical studies have indicated that the K2-PH domain is highly soluble and binds to phosphoinositides, including both PIP2 and PIP3 but preferentially PIP3 (20). To further investigate these interactions, we performed binding studies of the K2-PH to the head groups of PIP3 (IP4) and PIP2 (IP3), respectively, using chemical shift mapping. Supplemental Fig. S1 displays the well dispersed NMR spectrum of K2-PH in the presence of IP4 with the resonance assignments (*red color*). As compared with the free form K2-PH (*green color*), a selective number of residues were substantially perturbed upon K2-PH binding to IP4, suggesting that they are involved in PIP3 binding (supplemental Fig. S1). Fig. 1*B* displays the chemical shift perturbation profile of K2-PH by IP4. The IP4-induced chemical changes (Fig. 1*B*) are much larger than those induced by IP3 (Fig. 1*C*), indicating that PIP2 is a weaker ligand for K2-PH than PIP3, as consistent with previous biochemical and functional studies that PIP3 is a preferred ligand for K2-PH (20). Using the surface plasmon resonance (SPR) technique, we measured the K_D for K2-PH with IP4, which was estimated to be 2.12 ± 0.19 μM (Fig. 1*D*), in the similar range to other PH domains such as Gap1 PH binding to IP4 (K_D = ~0.35 μM) (28). The SPR signal of the IP3 binding to K2-PH was too small to be analyzed (not shown) but is consistent with the NMR data that IP3 is a significantly weaker ligand than IP4. Given that PI3K is critically involved in regulating kindlin-2 function and integrin activation (20) and that PIP2 is enriched in the inner membrane integrin site (22), our data support a model in which there is an enhanced kindlin-2/membrane association consequent to PI3K-mediated PIP2/PIP3 conversion.

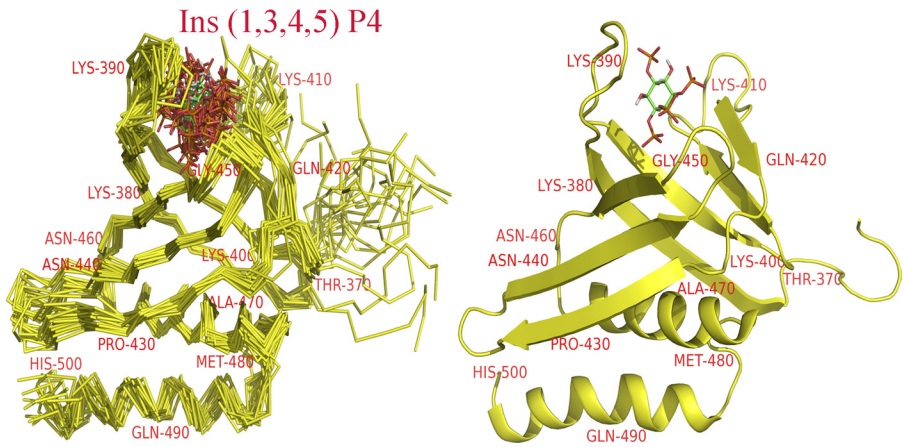

FIGURE 2. **Solution structure of the complex between the kindlin-2 PH domain and IP4.** *Left*, ensemble of 20 lowest energy structures of the kindlin-2 PH domain bound to IP4. *Right*, ribbon drawing of a representative structure of the kindlin-2 PH domain bound to IP4 (*Ins (1,3,4,5) P4*).

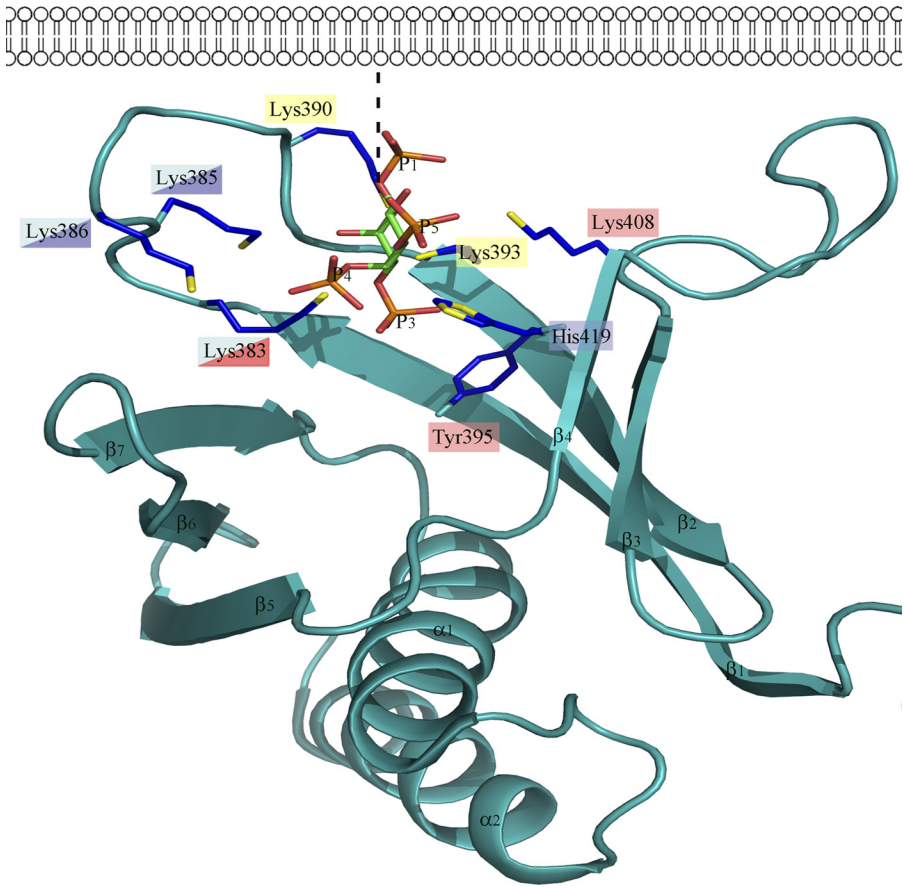

FIGURE 3. **K2-PH domain has a positively charged IP4 binding pocket.** Residues that have potential contacts with IP4 are *highlighted* and labeled. The phosphate groups on IP4 are also labeled. The *dotted line* indicates how the phosphate group 1 can be extended to the membrane by connecting to the acyl chain of PIP3. Note that Lys[383], Lys[385], and Lys[386] are labeled in *two colors*, indicating that they are involved in contacting more than one phosphate group, *i.e.* the 4- and 5-phosphate groups.

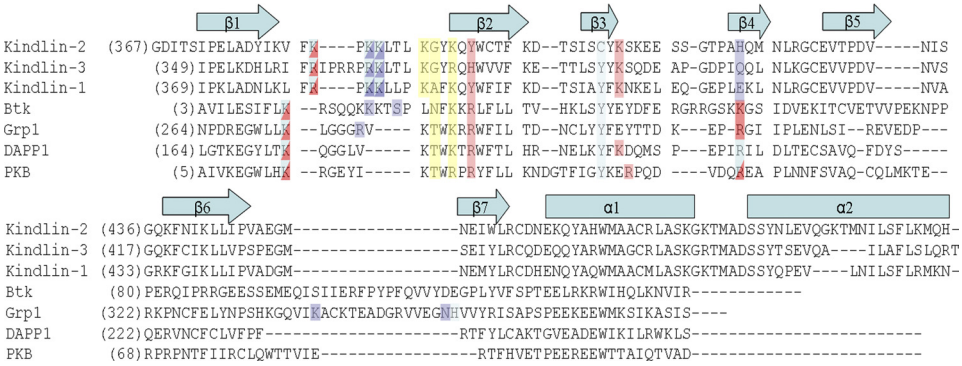

FIGURE 4. **Structure-based sequence alignment of K2-PH domain with other selective PH domain structures bound to IP4.** Residues involved in binding to different phosphate groups are colored differently: *yellow*, binding to the 1-phosphate group; *red*, binding to the 3-phosphate group; *light green*, binding to the 4-phosphate group; *blue*, binding to the 5-phosphate group. Note that the kindlin-1 alignment and IP4 binding site are proposed based on the sequence homology with kindlin-2, whereas others are all structure-based alignments. Also, some IP4 binding residues are marked by *two colors*, indicating that they are involved in interacting with more than one phosphate group (see also Fig. 3).

Structure Determination of the Kindlin-2 PH Domain Bound to IP4—To gain atomic insight into the K2-PH·PIP3 recognition, we set out to determine the structure of K2-PH in complex with IP4. The one-dimensional NMR spectrum of the bound IP4 is very similar to that of free IP4 (see supplemental Fig. S2) except that the H2 of the bound IP4 was more downfield-shifted, probably due to the interaction with K2-PH. The complete proton chemical shift assignments of the bound IP4 are provided in supplemental Table S1. Nineteen intermolecular NOEs between IP4 and K2-PH were assigned including nine unambiguous ones (supplemental Fig. S3). These NOEs allowed the total NMR structure of the K2-PH·IP4 complex to be calculated (see Table 1 for statistics). Fig. 2, *left*, displays the highly converged superposition of 20 lowest energy structures. The K2-PH domain consists of a seven-stranded β-sandwich core where two β-sheets consisting of four β-strands (β1-β4) and three β-strands (β5-β7) form a barrel-like structure (Fig. 2, *right*). One side of the barrel-like structure is capped by the

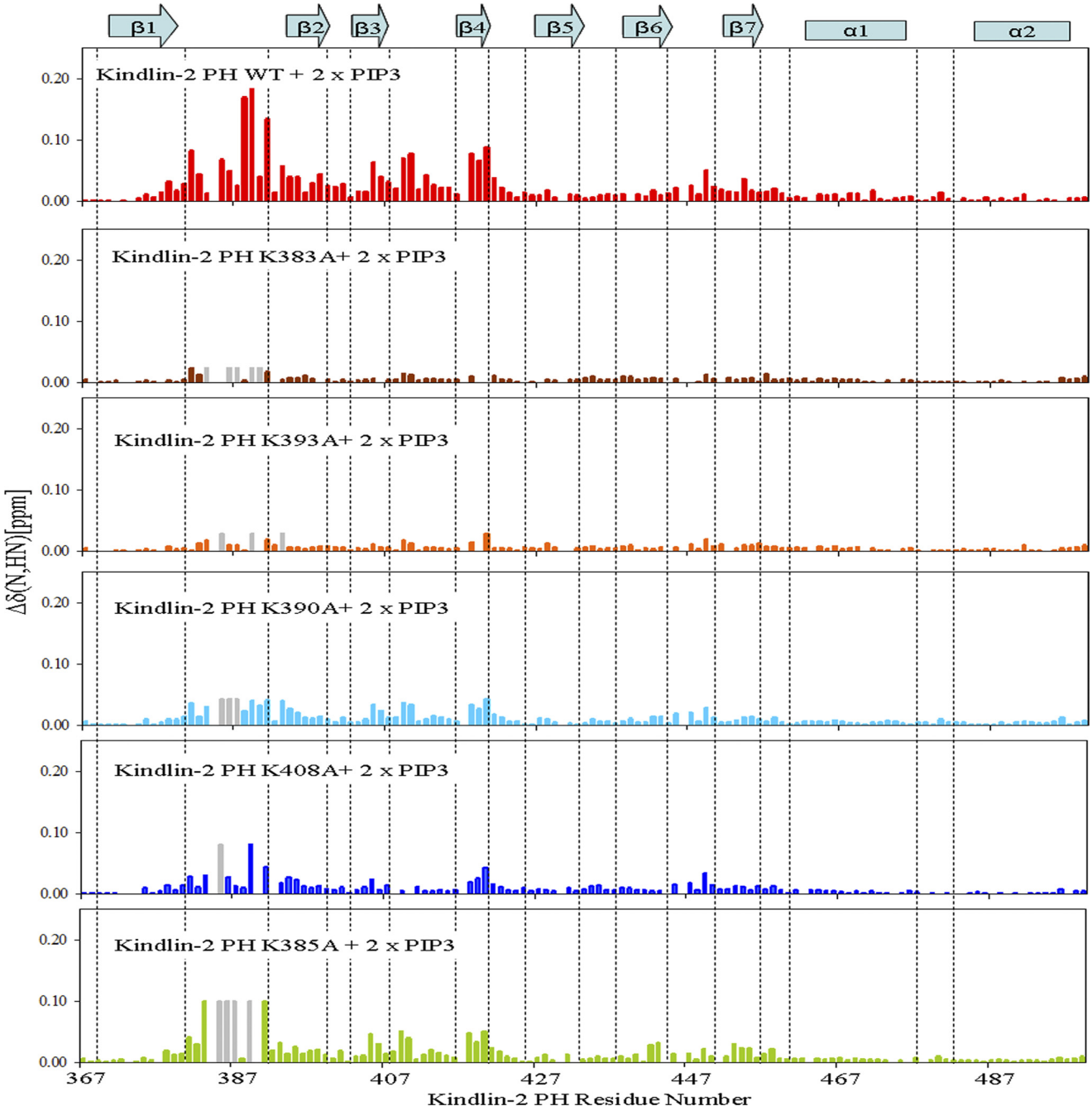

FIGURE 5. **Chemical shift perturbation profiles of wild type and mutant K2-PH with IP4.** *Gray bars* indicate line-broadening residues. The perturbation profiles were derived from the HSQC spectra of 0.1 mM ^{1}H-^{15}N-labeled wild type and mutant samples in the absence and presence of 0.2 mM IP4.

conserved α1 helix, but the opposite side is open and highly positively charged from a cluster of lysine residues, preserved for the phosphoinositide binding site (Fig. 3). Structural comparison using the program DALI (29) revealed that the K2-PH β-sandwich core is similar to those of other known PH domain structures bound to IP4 with root mean square differences between 2.6 and 3.1 Å for the equivalent C_α atom pairs, despite the low overall sequence identity (5–10%) with significant structural and sequence variations in the loop regions (β1-β2, β5-β6, and β6-β7) (supplemental Fig. S4). K2-PH has an additional helix (α2) at the C terminus that packs with α1 helix (Fig. 2, *right*, and supplemental Fig. S4) as compared with the canonical PH fold, and such packing seems to be important for the structural stability of K2-PH. The overall fold of K2-PH bound to IP4 is also similar to an NMR structure (Protein Data Bank (PDB) code 2YS3) of free form kindlin-3 PH (K3-PH) domain (55% identity, supplemental Fig. S5) with a root mean square difference of 2.3 Å for the equivalent C_α atom pairs. However, significant loop movement was observed in the IP4 binding site of K2-PH as compared with K3-PH (supplemental Fig. S5), suggesting that IP4 binding may induce some local conformational change, as consistent with the significant chemical shift changes of these loop residues in K2-PH upon binding to IP4 (Fig. 1*B* and supplemental Fig. S1).

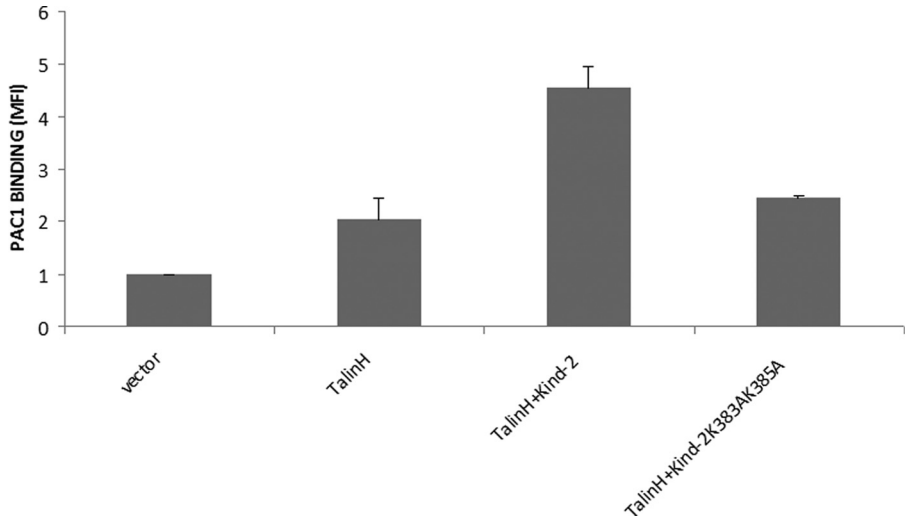

FIGURE 6. **Functional data showing that WT kindlin-2 but not the PIP3 binding-defective K383A/K385A mutant dramatically enhances the talin-mediated integrin activation.** The EGFP constructs for the two kindlin-2 forms were transfected into CHO cells stably expressing integrin $\alpha_{IIb}\beta_3$, and the activation of the integrin was monitored by flow cytometry with the activation-specific antibody PAC-1 (see "Experimental Procedures"). Based on flow cytometry and Western blots, the expression levels of the two kindlin-2 forms were similar. The experiments were repeated three times with the p value < 0.003 as compared with WT kindlin-2 and talin-H. *Error bars* indicate S.E. *MFI*, median fluorescence intensity.

Structural Basis of Phosphoinositide Recognition by the Kindlin-2 PH Domain—The IP4 ligand recognizes a binding pocket that is mostly formed by hyper-variable loop regions (β1-β2 and β3-β4) at the open end of the β-barrel like structure of the K2-PH domain (Fig. 3). The IP4 binding site of K2-PH is spatially similar to other known PH domains (supplemental Fig. S4), in which a cluster of positively charged residues contact the negatively charged phosphate groups of IP4, and therefore the ligand binding interface displays highly electrostatic complementarities. The specific potential contacts between IP4 and K2-PH are as follows. The 3-phosphate group of IP4 interacts with the side chains of Lys^{383} and Lys^{393} and the side chains of Tyr^{395} and His^{419} (Fig. 3). These interactions may account for the stronger binding of K2-PH to IP4 than IP3 (Fig. 1*B versus* Fig. 1*C*). The 4-phosphate group interacts with the side chains of Lys^{383}, Lys^{385}, and Lys^{386} that are clustered in a relatively long β1-β2 loop (8 residues, Fig. 3). The 5-phosphate group of IP4 interacts with the side chain of Lys^{408} and the polar side chain of His^{419} (Fig. 3). The Lys^{390} side chain is located at the entry of IP4 and contacts with the 1-phosphate group of IP4, which further connects the acyl chain of PIP3 to enter into membrane (Fig. 3). We note that although it is not technically feasible to experimentally detect direct NOEs between lysine ϵ-amino groups and phosphate groups of IP4 by NMR spectroscopy, the IP4 binding site and orientation in our structure are in full agreement with the experimental data for the following reasons. 1) The largest resonance perturbations upon IP4 binding occurred in the β1-β2 and β3-β4 loop regions that directly contact IP4 in our structure, which are consistent with the IP4 binding sites in other known PH domain structures (supplemental Fig. S4). 2) The side chain orientations of the IP4-perturbed Lys residues, Lys^{383}, Lys^{385}, Lys^{386}, Lys^{390}, Lys^{393}, and Lys^{408}, are well positioned to potentially coordinate the negatively charged phosphate groups of IP4 (Fig. 3), and mutation of each of them impairs the IP4 binding (see below). 3). Specific intermolecular NOEs were detected between the inositol sugar protons and hydrophobic side chains of some highly perturbed Lys residues by IP4.

Conventional PH domains with high affinity to phosphoinositides involve a signature motif consisting of conserved basic residues of KX_n(K/R)XR, where the initial lysine residue is located near the C terminus of the β1 strand, whereas the (K/R)XR motif is located near the N terminus of the β2 strand (30). Fig. 4 provides the representative examples of the Btk, Grp1, DAPP1, and PKB/Akt PH domains. As a comparison, the K2-PH domain seems to lack such motif with a sequence of Val^{381}-X_{11}-Lys^{393}-Gln^{394}-Tyr^{395} in the equivalent region (Fig. 4). However, our structure reveals that the side chain of Lys^{383}, located in the β1-β2 loop, spatially compensates the missing first conserved lysine of the conventional KX_m(K/R)XR motif. The side chains of Lys^{385} and Lys^{386} are in close proximity to Lys^{383} and also contribute to the binding to IP4 (Fig. 3). Thus, although K2-PH does not have a conventional IP4 binding motif, it contains a unique IP4 binding site clustered with positively charged residues, and this site appears to be well conserved among all three kindlin family members (Fig. 4).

Site-directed Mutagenesis and Functional Significance of the K2-PH/PIP3 Interaction—To evaluate the functional significance of the IP4 binding site in the K2-PH domain, we performed the site-directed mutagenesis experiments. We selected all 5 Lys residues, Lys^{383}, Lys^{385}, Lys^{390}, Lys^{393}, and Lys^{408}, that are involved in binding to IP4 in our structure (Fig. 3) and generated the single point mutants of each of the 5 lysine residues to alanines. Each mutant was found to fold similarly as the wild type, as judged by gel filtration and HSQC spectra data (not shown), demonstrating that the mutations on these surface residues did not affect the overall structural integrity of the K2-PH domain. We then examined the interaction of each K2-PH mutant with IP4 by chemical shift mapping. These mutants had either diminished (K383A, K393A) or significantly reduced chemical shift changes (Lys^{390}, Lys^{385}, and Lys^{408}) as compared with that for WT (Fig. 5), thus providing cross-vali-

dation of the IP4 binding pocket from our structure and the importance of these residues in recognizing PIP3.

Next, we determined how phosphoinositide binding would affect the kindlin-2 function. Although previous studies suggested that the PIP3 binding to the K2-PH domain may regulate integrin activation (20), it is unclear whether such binding controls the integrin co-activating activity of kindlin-2 with talin, a major pathway for kindlin-2 to regulate integrin activation (12–14). Based on the point mutation data in Fig. 5, we mutated 2 spatially close Lys residues, Lys^{383} and Lys^{385}, into Ala, which should maintain the three-dimensional fold of K2-PH but dramatically reduce the K2-PH binding to PIP3. Fig. 6 shows that although wild type kindlin-2 cooperates with talin to activate integrin $\alpha_{IIb}\beta_3$, such co-activation was substantially reduced by K383A/K385A mutation, thus providing strong functional evidence that the phosphoinositide binding to kindlin-2 is crucial for the kindlin-2 co-activator function.

DISCUSSION

Phosphoinositide-mediated protein targeting to the inner membrane of cells is a common and crucial mechanism for localization and functional regulation of many membrane-associated proteins. Among all phosphoinositides, PIP2, enriched in the inner membrane surface, binds to numerous protein domains including the FERM domain of radixin (31), ezrin (32), and talin (33, 34). Radixin and ezrin FERM domains bind to PIP2 via the interface between their F1 and F3 domains (31, 32), whereas the talin FERM domain appears to utilize distinct positively charged regions on both F2 and F3 for PIP2 binding (34). Here we showed quantitatively that kindlin-2 binds PIP2 as well as PIP3 via an unusual PH domain contained within its FERM domain (Fig. 1). This phosphoinositide binding mode to kindlin is clearly different from that in radixin, ezrin, and talin, although talin FERM domain has an integrin binding F3 subdomain very similar to that of kindlin-2. Detailed structural analysis revealed that the K2-PH domain has a distinct positively charged PIP3 binding pocket well conserved in kindlins and that multiple contacts between the 3-phosphate of PIP3 and K2-PH also explain why K2-PH has higher affinity for PIP3 than PIP2. Given that PI3K is crucially involved in the kindlin-2-mediated integrin activation (20), our results support a dynamic model where PI3K, upon activation, converts PIP2 to PIP3, thereby resulting in an enhanced membrane association of kindlin-2. Such membrane association is clearly important for kindlin-2 function because disruption of the phosphoinositide binding dramatically impairs the ability of kindlin-2 to regulate integrin activation (Fig. 6).

How does kindlin-2 cooperate with talin to induce synergistic integrin activation? Our functional data indicate that such cooperation relies on the PH domain-mediated membrane association of kindlin-2. Interestingly, the talin FERM domain also binds to membrane, and the binding is important for stabilizing the talin-integrin interaction (34–36). It is thus conceivable that the kindlin-2 PH domain-mediated membrane association may also stabilize the kindlin-2 binding to integrin β CT. Because talin and kindlin-2 (12, 13) bind to different sites of integrin β CT via their F3 subdomains, the membrane anchoring of both talin and kindlin-2 may promote a fully stabilized integrin conformation in its activated state, explaining why both are required to optimize integrin activation.

Kindlin-2 is highly homologous to other kindlin family members including kindlin-1 and kindlin-3. Our analysis of the PIP3 binding to K2-PH reveals that the recognition mode is likely conserved in all kindlin members, thus suggesting a common mechanism for the kindlin membrane localization via PI3K-mediated PIP3 targeting.

In summary, we have undertaken a detailed biochemical, structural, and functional analysis of the kindlin-2 PH domain that confers a distinct membrane anchoring capability of the kindlin-2 FERM domain. Our results revealed a novel phosphoinositide recognition mode of the PH domain, providing important molecular insight into how it regulates the membrane targeting of kindlin-2 and facilitates the talin-mediated integrin activation.

Acknowledgments—We thank Drs. Jun Yang and Satya P. Yadav for technical assistance.

REFERENCES

1. Hynes, R. O. (2002) *Cell* **110,** 673–687
2. Calderwood, D. A. (2004) *J. Cell Sci.* **117,** 657–666
3. Qin, J., Vinogradova, O., and Plow, E. F. (2004) *PLoS Biol.* **2,** e169
4. Ma, Y. Q., Qin, J., and Plow, E. F. (2007) *J. Thromb. Haemost.* **5,** 1345–1352
5. Vinogradova, O., Velyvis, A., Velyviene, A., Hu, B., Haas, T., Plow, E., and Qin, J. (2002) *Cell* **110,** 587–597
6. Kim, M., Carman, C. V., and Springer, T. A. (2003) *Science* **301,** 1720–1725
7. Ma, Y. Q., Yang, J., Pesho, M. M., Vinogradova, O., Qin, J., and Plow, E. F. (2006) *Biochemistry* **45,** 6656–6662
8. Kim, C., Lau, T. L., Ulmer, T. S., and Ginsberg, M. H. (2009) *Blood* **113,** 4747–4753
9. Shi, X., Ma, Y. Q., Tu, Y., Chen, K., Wu, S., Fukuda, K., Qin, J., Plow, E. F., and Wu, C. (2007) *J. Biol. Chem.* **282,** 20455–20466
10. Moser, M., Nieswandt, B., Ussar, S., Pozgajova, M., and Fässler, R. (2008) *Nat. Med.* **14,** 325–330
11. Moser, M., Bauer, M., Schmid, S., Ruppert, R., Schmidt, S., Sixt, M., Wang, H. V., Sperandio, M., and Fässler, R. (2009) *Nat. Med.* **15,** 300–305
12. Ma, Y. Q., Qin, J., Wu, C., and Plow, E. F. (2008) *J. Cell Biol.* **181,** 439–446
13. Montanez, E., Ussar, S., Schifferer, M., Bösl, M., Zent, R., Moser, M., and Fässler, R. (2008) *Genes Dev.* **22,** 1325–1330
14. Harburger, D. S., Bouaouina, M., and Calderwood, D. A. (2009) *J. Biol. Chem.* **284,** 11485–11497
15. Malinin, N. L., Zhang, L., Choi, J., Ciocea, A., Razorenova, O., Ma, Y. Q., Podrez, E. A., Tosi, M., Lennon, D. P., Caplan, A. I., Shurin, S. B., Plow, E. F., and Byzova, T. V. (2009) *Nat. Med.* **15,** 313–318
16. Svensson, L., Howarth, K., McDowall, A., Patzak, I., Evans, R., Ussar, S., Moser, M., Metin, A., Fried, M., Tomlinson, I., and Hogg, N. (2009) *Nat. Med.* **15,** 306–312
17. Tu, Y., Wu, S., Shi, X., Chen, K., and Wu, C. (2003) *Cell* **113,** 37–47
18. Plow, E. F., Qin, J., and Byzova, T. (2009) *Curr. Opin. Hematol.* **16,** 323–328
19. Moser, M., Legate, K. R., Zent, R., and Fässler, R. (2009) *Science* **324,** 895–899
20. Qu, H., Tu, Y., Shi, X., Larjava, H., Saleem, M. A., Shattil, S. J., Fukuda, K., Qin, J., Kretzler, M., and Wu, C. (2011) *J. Cell Sci.* **124,** 879–891
21. Kolanus, W., and Seed, B. (1997) *Curr. Opin. Cell Biol.* **9,** 725–731
22. Ling, K., Schill, N. J., Wagoner, M. P., Sun, Y., and Anderson, R. A. (2006) *Trends Cell Biol.* **16,** 276–284
23. Clore, G. M., and Gronenborn, A. M. (1998) *Trends Biotechnol.* **16,** 22–34
24. Delaglio, F., Grzesiek, S., Vuister, G. W., Zhu, G., Pfeifer, J., and Bax, A. (1995) *J. Biomol. NMR* **6,** 277–293

25. Rieping, W., Habeck, M., Bardiaux, B., Bernard, A., Malliavin, T. E., and Nilges, M. (2007) *Bioinformatics* **23,** 381–382
26. Cornilescu, G., Delaglio, F., and Bax, A. (1999) *J. Biomol. NMR.* **13,** 289–302
27. Schwieters, C. D., Kuszewski, J. J., Tjandra, N., and Clore, G. M. (2003) *J. Magn. Reson.* **160,** 65–73
28. Fukuda, M., and Mikoshiba, K. (1996) *J. Biol. Chem.* **271,** 18838–18842
29. Holm, L., Kääriäinen, S., Rosenström, P., and Schenkel, A. (2008) *Bioinformatics* **24,** 2780–2781
30. DiNitto, J. P., Cronin, T. C., and Lambright, D. G. (2003) *Sci. STKE* **2003,** re16
31. Hamada, K., Shimizu, T., Matsui, T., Tsukita, S., and Hakoshima, T. (2000) *EMBO J.* **19,** 4449–4462
32. Blin, G., Margeat, E., Carvalho, K., Royer, C. A., Roy, C., and Picart, C. (2008) *Biophys. J.* **94,** 1021–1033
33. Goksoy, E., Ma, Y. Q., Wang, X., Kong, X., Perera, D., Plow, E. F., and Qin, J. (2008) *Mol. Cell* **31,** 124–133
34. Saltel, F., Mortier, E., Hytönen, V. P., Jacquier, M. C., Zimmermann, P., Vogel, V., Liu, W., and Wehrle-Haller, B. (2009) *J. Cell Biol.* **187,** 715–731
35. Martel, V., Racaud-Sultan, C., Dupe, S., Marie, C., Paulhe, F., Galmiche, A., Block, M. R., and Albiges-Rizo, C. (2001) *J. Biol. Chem.* **276,** 21217–21227
36. Anthis, N. J., Wegener, K. L., Ye, F., Kim, C., Goult, B. T., Lowe, E. D., Vakonakis, I., Bate, N., Critchley, D. R., Ginsberg, M. H., and Campbell, I. D. (2009) *EMBO J.* **28,** 3623–3632